



A Highly Active, CO₂-tolerant Electrode for Oxygen Reduction Reaction

Journal:	<i>Energy & Environmental Science</i>
Manuscript ID	EE-ART-04-2018-001140.R1
Article Type:	Paper
Date Submitted by the Author:	03-Jun-2018
Complete List of Authors:	<p>Chen, Yu; Georgia Institute of Technology, School of Materials Science and Engineering</p> <p>Yoo, Seonyoung; Georgia Institute of Technology, School of Material Science & Engineering</p> <p>Choi, yongman; Georgia Institute of Technology, Materials Science and Engineering</p> <p>Kim, Jun; Georgia Institute of Technology, School of Materials Science and Engineering</p> <p>Ding, Yong; Georgia Institute of Technology, School of Materials Science and Engineering</p> <p>Pei, Kai; Georgia Institute of Technology, School of Materials Science and Engineering</p> <p>Murphy, Ryan; Georgia Institute of Technology, School of Materials Science and Engineering</p> <p>Zhang, Yanxiang; Harbin Institute of Technology, School of Materials Science and Engineering</p> <p>Zhao, Bote; Georgia Institute of Technology, School of Materials Science & Engr</p> <p>Zhang, Weilin; Georgia Institute of Technology, School of Materials Science and Engineering</p> <p>Chen, Huijun; South China University of Technology, School of Environment and Energy</p> <p>Chen, Yan; South China University of Technology, School of Environment and Energy</p> <p>Yuan, Wei; Georgia Institute of Technology, School of Materials Science and Engineering</p> <p>Yang, Chenghao; South China University, School of Environment and Energy; South China University of Technology, Key Laboratory of Fuel Cell Technology of Guangdong Province</p> <p>Liu, Meilin; Georgia Institute of Technology, School of Materials Science and Engineering</p>

A Highly Active, CO₂-tolerant Electrode for Oxygen Reduction Reaction

Yu Chen¹, Seonyoung Yoo¹, YongMan Choi², Jun Hyuk Kim¹, Yong Ding¹, Kai Pei¹, Ryan Murphy¹, Yanxiang Zhang³, Bote Zhao¹, Weilin Zhang¹, Huijun Chen⁴, Yan Chen⁴, Wei Yuan¹, Chenghao Yang⁴, and Meilin Liu^{1*}

¹School of Materials Science and Engineering, Georgia Institute of Technology, 771 Ferst Dr NW, Atlanta, GA, 30332-0245, US

²SABIC Technology Center, Riyadh 11551, Saudi Arabia

³National Key Laboratory for Precision Hot Processing of Metals, School of Materials Science and Engineering, Harbin Institute of Technology, Harbin, Heilongjiang 150001, China

⁴Guangzhou Key Laboratory for Surface Chemistry of Energy Materials, New Energy Research Institute, School of Environment and Energy, South China University of Technology, Guangzhou 510006, China

*Corresponding author: meilin.liu@mse.gatech.edu

Keywords: Solid oxide fuel cells; perovskite; oxygen reduction reaction; CO₂ tolerance; cathode materials

Abstract: One challenge facing the development of high-performance cathode for solid oxide fuel cells (SOFC) is the fast degradation rate of cathodes due to poisoning of contaminants commonly encountered in ambient air such as CO₂. Here we report a double perovskite PrBa_{0.8}Ca_{0.2}Co₂O_{5+δ} (PBCC) cathode with excellent ORR activity and remarkable CO₂ tolerance under realistic operation conditions. When tested in a symmetrical cell in air with ~1 v% CO₂ at 750 °C, the PBCC electrode shows an area specific resistance of ~0.024 Ω cm², which increases to 0.028 Ω cm² after 1,000 h operation. The degradation rate is ~1/24 of that of the state-of-the-art La_{0.6}Sr_{0.4}Co_{0.2}Fe_{0.8}O₃ (LSCF) cathode under the same conditions. Impedance spectroscopy and *in situ* surface enhanced Raman spectroscopy analyses indicate that the surface of PBCC electrode is much more active for oxygen exchange and more robust against CO₂ than that of LSCF, as confirmed by density functional theory calculations. The fast ORR kinetics and excellent durability of PBCC in air with CO₂ highlight the potential of PBCC as a highly

promising material for devices involving oxygen electrochemistry such as solid oxide fuel cells, electrolysis cells, or gas separation membranes.

Broader context

Perovskite materials with excellent ionic and electronic conductivity have been extensively studied as electrodes for efficient energy conversion and storage. They are ideally suited for electrochemical applications that involve oxygen electrochemistry such as fuel cells and membrane reactors. To make them economically competitive and commercially viable, however, several materials challenges must be overcome. One of them is to significantly enhance the durability against contaminants in ambient air while maintaining high electro-catalytic activity under operating conditions. Here we report the rational design of a high-performance electrode with excellent durability when exposed to ambient air containing ~1% CO₂. Further, the concept and the materials developed may be applicable to other chemical and energy transformation processes, including metal-air batteries, electrolyzers, dye-sensitized solar cells, and photocatalysis.

Introduction

Regenerative solid oxide fuel cells (SOFCs) have potential to be the most attractive option for efficient energy storage and conversion; they can also serve as an economic bridge for transition from the fossil-fuel to the hydrogen-fuel economy because of the excellent fuel flexibility^{1, 2}. However, the cathodes of SOFCs still contribute the most to degradation in performance and efficiency loss in the existing systems^{3, 4}. One technical opportunity is to dramatically enhance the durability of the cathode while maintaining high electro-catalytic activity for oxygen reduction reaction (ORR) in order to reduce the cost and prolong the operational lifetime⁵⁻⁸.

La_xSr_{1-x}Co_yFe_{1-y}O_{3-δ} (LSCF)-based perovskite materials have been extensively investigated as electrodes for high-temperature electrochemical devices due to its excellent ionic

and electronic conductivity and good ORR activity in the temperature range of 600-800°C⁹. One shortcoming for an LSCF electrode is that its ORR activity is likely limited by the sluggish surface exchange process rather than the bulk charge transport process^{10, 11}. Another technical barrier for an LSCF electrode is its poor durability due to Sr enrichment or segregation to the surface^{6, 12}, caused by electrostatic attraction of the positively charged oxygen vacancies enriched at the surface¹³. The Sr-enrichment may induce the formation of secondary phases such as SrCO₃, Sr(OH)₂, or SrCrO₄, which are detrimental to the surface electro-catalytic activity for ORR, leading to continuous degradation in electrode performance¹⁴⁻¹⁶.

Accordingly, extensive efforts have been devoted to the development of new cathode structures and materials with enhanced ORR activity¹⁷⁻¹⁹, improved surface stability^{13, 20} and good tolerance against contaminants poisoning²¹. For instance, Jiang *et al.* demonstrated the feasibility and effectiveness of enhancing Cr-poisoning by surface modification of the cathode with a coating of a simple oxide like BaO or a mixture of two phases such as yttria stabilized zirconia (YSZ) and doped ceria²²⁻²⁴. Recently, Liu *et al.* developed a unique surface modification of LSCF cathode by deposition of conformal coatings *via* one-step infiltration; the coatings can suppress surface Sr segregation, thus further enhancing the durability or tolerance to contaminants poisoning^{12, 16, 25}. Recently, a cathode with high tolerance to air with 10%CO₂ has been reported²⁶; a three-dimensional (3D) hierarchical CO₂-protective shell was deposited on Ba_{0.5}Sr_{0.5}Co_{0.8}Fe_{0.2}O₃ (BSCF) cathode through infiltration followed by microwave plasma treatment. The hierarchical shell consisted of a dense thin-film substrate with cones on the top of the substrate. A single cell with this cathode demonstrated a power density of ~0.7Wcm⁻² at a cell voltage of 0.7V at 700°C in air with 10%CO₂ (within 1 h). However, the cells were tested in CO₂-containing atmosphere for only 1 h. Long-term stability is vital to practical applications

since SOFCs are supposed to run for thousands of hours. Also, it is noted that the cathode fabrication process is relatively complex to obtain the desired structure: multistep solution infiltration, firing, and microwave plasma treatment, which might not be applicable for large scale SOFCs.

While surface modification is effective, it is critical to develop cathode materials that are inherently tolerant to degradation or contaminant poisoning. For example, Sr-free cathode materials have been extensively studied. Perovskite, Aurivillius oxide based cathode ($\text{Bi}_2\text{Sr}_2\text{Nb}_2\text{MnO}_{12-d}$)²⁷, or Ruddlesden-Popper (RP) perovskite-like materials (such as $\text{La}(\text{Ni},\text{Fe})\text{O}_{3-\delta}$, Nd_2NiO_4 and Pr_2NiO_4) were thus proposed and studied as candidate cathode materials for SOFCs^{28, 29}. For instance, a new cathode composed of Ag, $\text{Sm}_{0.2}\text{Ce}_{0.8}\text{O}_2$, and $\text{Bi}_2\text{Sr}_2\text{Nb}_2\text{MnO}_{12-d}$ was developed²⁷, demonstrating good stability in air containing 10% CO_2 in symmetrical cells at 700 °C for only 5 h. However, the single cell performance in air with CO_2 was not shown, and there was no data on long-term stability of the cells in air containing CO_2 . To date, unfortunately, none of these new cathode materials have sufficient durability under realistic operating conditions. In addition, the mechanism of CO_2 tolerance is still unknown; mechanistic understanding is vital to achieving rational design of new materials and electrode structures tolerant to CO_2 poisoning.

Here we report a layered double perovskite material $\text{PrBa}_{0.8}\text{Ca}_{0.2}\text{Co}_2\text{O}_{5+\delta}$ (PBCC), demonstrating high ORR activity and excellent durability in air containing CO_2 under typical SOFCs operation conditions. An anode-supported single cell with the PBCC cathode achieved a power density of $\sim 0.7 \text{ W cm}^{-2}$ at 700 °C under a cell voltage of 0.7 V for ~ 220 h when a simulated air with $\sim 1\%$ CO_2 was used as oxidant and humidified H_2 ($\sim 3\%$ H_2O) as fuel. Careful characterization and analyses indicate that the surface of the PBCC electrode is much more

active for ORR and robust against CO₂ than that of LSCF, suggesting that PBCC is a highly promising cathode material for low-cost, high-performance, and durable SOFCs. The mechanism of the remarkable CO₂ tolerance of PBCC under realistic operation conditions has been unravelled using *in situ* SERS, impedance spectroscopy, and DFT calculations, providing information vital to achieving rational design of more efficient and durable cathodes for solid oxide fuel cells.

Results and Discussion

Structure of PBCC

Shown in **Figure 1a** is a schematic view of the crystal structure of PBCC as confirmed by XRD refinement (**Figure 1b**), with a stacking sequence of Ba(Ca)O/CoO_x/PrO_x/CoO_x/Ba(Ca)O. Shown in **Figure 1c** is a high-angle annular dark-field (HAADF) image of a PBCC grain, recorded with electron beam along the [100] direction. The inset is the corresponding fast Fourier transform (FFT) pattern. The observation of the superlattice spots (due to the difference in atomic number of ordered A-site cations) in the FFT patterns (insets) confirms the double perovskite structure of PBCC with Pr and Ba(Ca) cations ordered in alternating layers along the c axis, i.e., with a stacking sequence of [Ba(Ca)O]–[CoO₂]–[PrO]–[CoO₂]–[Ba(Ca)O]. Moreover, the layered structure can be observed clearly through the line scan (brightness) along the red line in **Figure 1c**. The intensity difference shown in **Figure 1d** clearly confirmed the layered structure. The distance between PrO or BaO planes is about 0.76 nm, consistent with XRD analysis. Such a layered structure is vital to rapid transport of oxygen vacancies and fast surface exchange of oxygen³⁰⁻³⁴. For instance, PrBaCo₂O_{5+δ} (PBCO)-based material offered faster oxygen ion diffusion and surface-exchange kinetics than LSCF³⁵. Dissociated oxygen species can diffuse through the pore channels within PBCC bulk phase, as depicted earlier³². Ca doping

at the A site can suppress surface segregation of A-site cations, resulting in better long-term stability of the cathode^{13, 30}.

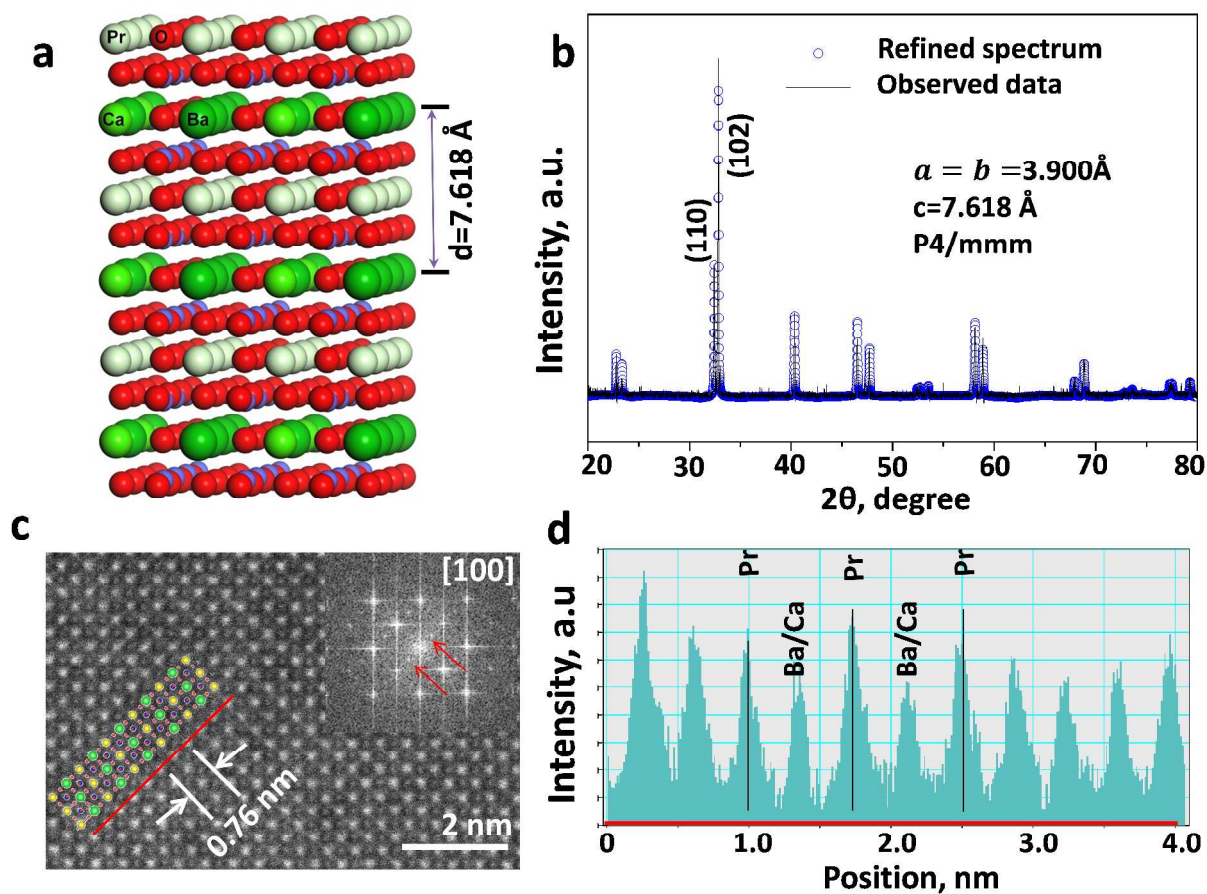


Figure 1 Crystalline Structure of PBCC. (a) Schematics of PBCC crystal structure; (b) Refined XRD profiles of PBCC (powder sample) after fired in air at 1000°C for 2h; and (c) High resolution STEM image of PBCC lattice. The red arrow indicated the super-lattice structure; and (d) Line scan profile (brightness) along the red line in (c).

Electrochemical performance of PBCC in air

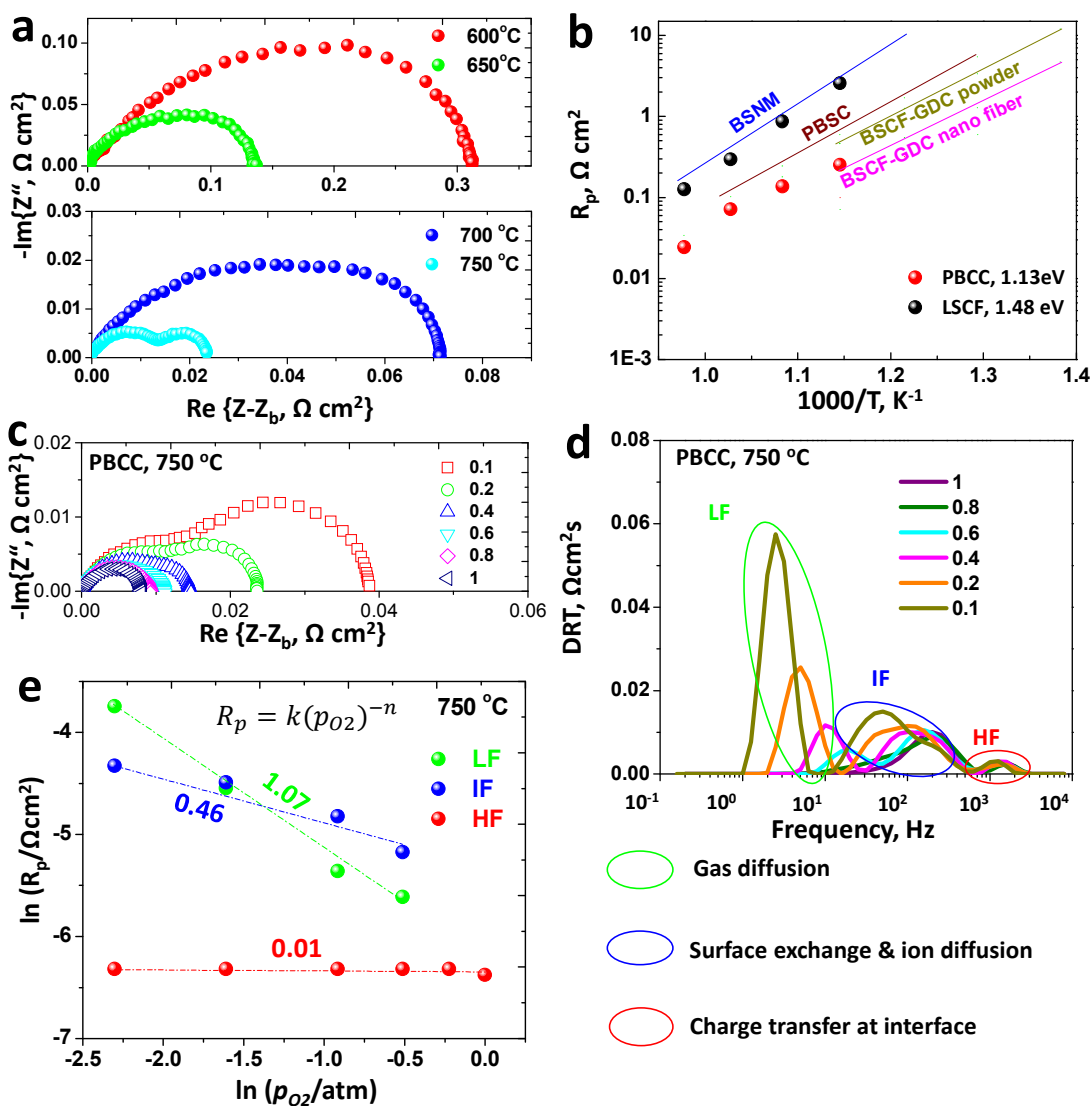


Figure 2 EIS and the analyses using DRT. (a) EIS of symmetrical cells with PBCC as electrode in ambient air; (b) Temperature dependence of interfacial polarization resistance (R_p) of PBCC (red ball) and LSCF (black ball). R_p of some high performing cathodes such as BSNM²⁷, PBSC³⁶, and BSCF-GDC powder and nanofiber³⁷, were also added for comparison. PBCC shows lower activation energy (1.13 eV) than LSCF (1.48 eV), indicating a less energy barrier for reaction; EIS (c) and distribution of relaxation time (DRT) (d) of PBCC as a function of oxygen partial pressure; (e) Dependence of each R_p as a function of p_{O_2} .

Shown in **Figure 2a** are some typical electrochemical impedance spectra (EIS) of the PBCC cathode determined using symmetrical cells with a configuration of PBCC | SDC | PBCC in ambient air at 600-750 °C. Interfacial polarization resistance (R_p) of PBCC is much lower than

that of LSCF cathode. For instance, R_p of PBCC in air at 750 °C is $\sim 0.024 \text{ } \Omega\text{cm}^2$, about 1/5 of that of LSCF ($0.13 \text{ } \Omega\text{cm}^2$) under the same conditions³. PBCC electrode shows much faster surface exchange kinetics and higher bulk diffusion coefficient than LSCF (**Figure S1**). The performance of the PBCC cathode reported here (**Figure 2b**) is comparable to those of the best cathodes with reasonable stability reported recently, including $\text{Bi}_2\text{Sr}_2\text{Nb}_2\text{MnO}_{12-\delta}$ (BSNM)²⁷, $\text{PrBa}_{0.5}\text{Sr}_{0.5}\text{Co}_2\text{O}_{5+\delta}$ (PBSC)³⁶ or BSCF-Gd_{0.1}Ce_{0.9}O_{2- δ} (GDC) nanofiber or mixture³⁷.

We have further investigated into the kinetics of the PBCC cathode by measuring the impedance spectra at different oxygen partial pressure (p_{O_2}) as shown in **Figure 2c**. The spectra were analyzed using distribution of relaxation time (DRT), a powerful tool for deconvoluting complex impedance data in order to separate or isolate some key steps involved in the electrode reactions³⁸. The characteristic frequency of a process is inversely proportional to the relaxation time of the electrode process. Thus, the lower the characteristic frequency, the longer the characteristic relaxation time of the electrode process. Thus, a down-shifting of the characteristic frequency for a specific process when the electrode is exposed to a contaminant (e.g., CO₂) may indicate degradation in kinetics of the electrode process (e.g., surface reaction) due to contaminant poisoning. Shown in **Figure 2d** are the DRT plots of PBCC at different oxygen partial pressure (p_{O_2}). Each plot has a set of three distinct peaks; denoted as low frequency (LF), intermediate frequency (IF), and high frequency (HF), corresponding to at least three distinct electrochemical processes. The integral area under each peak represents the resistance of the process³⁹. The general dependence of R_p on p_{O_2} can be approximated by the equation $R_p = k(p_{O_2})^{-n}$.

Shown in **Figure 2e** is the dependence of each R_p on the oxygen partial pressure. The number adjacent to each line is the n value for each process. n of 1.07 for the peak at LF

indicates that the LF peak corresponds to the impedance to mass transfer;⁴⁰ while $n = 0.46$ for the IF peak indicates that the IF peak is likely associated with the dissociation of O_2 to $2O_{ads}$ ⁴¹⁻⁴³. The insensitivity of the HF peaks has little dependence on p_{O_2} ($n = 0.01$), suggesting that the high-frequency process is likely associated with O^{2-} transfer across the electrode/electrolyte interface⁴⁴. The individual steps of the ORR process involved here may have different sensitivity to the contaminant such as CO_2 . Thus, analysis of impedance spectra using DRT may help us to gain more insights into the degradation mechanism, as to be elaborated below.

Durability of PBCC in air with CO_2

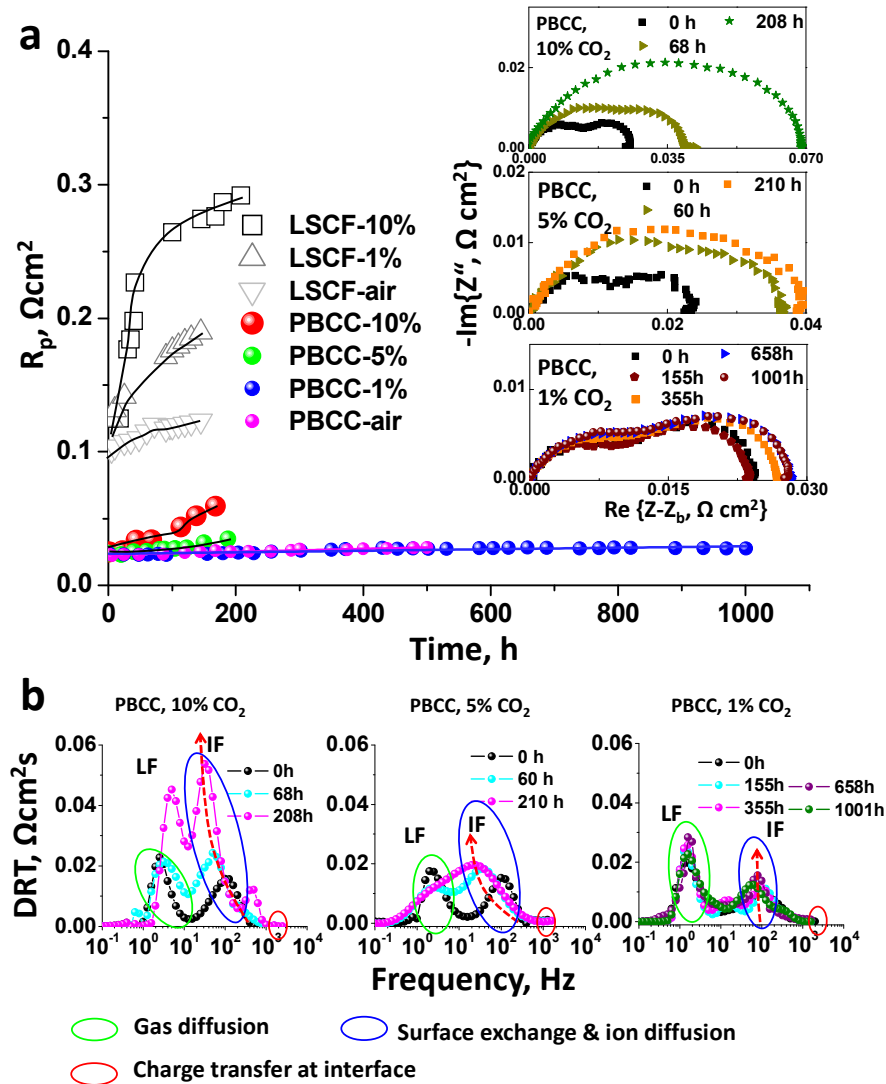


Figure 3 Durability of PBCC in air containing different amount of CO_2 . (a) Durability of PBCC and LSCF cathode in various concentration of CO_2 under OCV conditions. Insets are the EIS of PBCC in different concentration of CO_2 : 10% (top), 5% (middle) and 1% (bottom); and (b) DRT plots of PBCC cathodes at different testing time under OCV conditions in air with different concentration of CO_2 (10 vol%, 5vol% and 1 vol%).

In addition to high electro-catalytic activity for ORR, excellent durability of SOFC cathode is vital to commercialization of SOFC technology, especially when exposed to contaminants commonly encountered in ambient air such as CO_2 . Shown in **Figure 3a** is the summary of the durability of PBCC and LSCF cathodes in air with different concentrations of CO_2 . The insets are the electrochemical impedance spectra of the PBCC electrodes determined using a symmetrical cell immersed in air with different concentrations of CO_2 as a function of

testing time. Clearly, the impedance of the LSCF electrode increased significantly with time in air containing CO₂; the degree of degradation increased with the concentration of CO₂. In contrast, the impedance of the PBCC electrode displayed much better stability under the same testing conditions. For example, the impedance of the PBCC electrode remained relatively constant when the concentration of CO₂ was about 1%, consistent with the XRD analyses (**Figure S2**). When the concentration of CO₂ was increased to 5% and 10%, the PBCC electrode did degrade, but at a much slower deterioration rate than the LSCF electrodes.

In order to gain some insight into the detailed electrochemical process evolution (as a function of operation time) of the PBCC electrode in air with CO₂, we have also analyzed the impedance spectra using DRT (**Figure 3b**). Similar to earlier analysis, it appears that at least three processes (dispersed in the frequency domain) contributed to the electrode impedance; they occurred at LF (mass transfer near the interface), IF (surface exchange processes), and HF (charge transfer). It seems that the characteristic frequency of the IF peaks shifted to lower frequencies when the PBCC electrode was exposed to air containing high concentrations of CO₂ (5% or 10%), and the corresponding integral resistance increased continuously with time. Both changes suggest that high concentration CO₂ may deactivate the surface exchange process (IF), but has little effect on the other two processes at LF and HF. However, when the CO₂ concentration is 1 %, the characteristic frequency and the resistance of the surface exchange process (IF) remained relatively constant, an indication of robust surface properties of the PBCC against poisoning of up to ~1% CO₂.

Electrochemical performance of PBCC cathode in single cells

To demonstrate the high ORR activity and excellent CO₂-tolerance of the PBCC cathode in an actual fuel cell, we constructed a single cell using Ni-BaZr_{0.1}Ce_{0.7}Y_{0.1}Yb_{0.1}O₃ (BZCYYb)

as the anode support ($\sim 700\mu\text{m}$ thick), a SDC electrolyte ($\sim 30\mu\text{m}$ thick), and the PBCC cathode ($\sim 20\mu\text{m}$ thick). Cross-sectional views of cell components are shown in **Figure 4a and 4b**. The test cells were evaluated in a homemade setup (**Figure S3**), where simulated air with different concentrations of contaminants can be readily controlled. Shown in **Figure 4c and 4d** are some typical *I/P* curves and electrochemical impedance spectra of the single cells tested at 600-750 °C when humidified H_2 (with $\sim 3\%$ H_2O) was used as fuel and air as oxidant. At 700 °C, a peak power density of $\sim 0.949 \text{ W cm}^{-2}$ was achieved, which is higher than that of the single cells with an LSCF cathode (0.76 W cm^{-2})⁴⁵ and comparable to the best performance ever reported (see **Table 1**)⁴⁶, demonstrating the remarkable electro-catalytic activity of the PBCC cathode under realistic operating conditions (ROC). It is noted that the OCVs of our cells are higher than those of the cells using a ceria-based electrolyte reported by others⁵, due largely to the formation of an electron-blocking layer on the surface of the SDC electrolyte during co-firing of the electrolyte and Ni-BZCYYb anode at high temperatures.^{45, 47} Shown in **Figure 4e** is the long-term stability of the cell at a cell voltage of 0.7 V at 700 °C using humidified H_2 (with $\sim 3\%$ H_2O) as fuel and dry air or air with $\sim 1\%$ CO_2 as oxidant. The flow rate of the oxidant was controlled at 100 sccm. After the cell was operated for $\sim 50\text{h}$ (black line), the oxidant was switched from clean air to air containing $\sim 1\%$ CO_2 (red line). As seen, the performance of the cell with the PBCC cathode showed stable power output, demonstrating excellent CO_2 tolerance, which is consistent with our symmetrical cell measurements. It is well accepted that long-term stability is vital to practical applications since SOFCs are supposed to run for thousands of hours. Although some of the cathodes have been reported to have good tolerance to CO_2 poisoning in symmetrical cells^{26, 27}, the lack of long-term durability (over hundreds hour operation) of single cells may indicate that more development of the cathodes is still needed for real application. Also, it is noted that

the fabrication process and the composition of cathodes are relatively complex to obtain the desired structure: multi-step solution infiltration, firing, and microwave plasma treatment²⁶. In our case, the cathode is fabricated by a solution combustion method, which is simple and widely used by others⁴⁸.

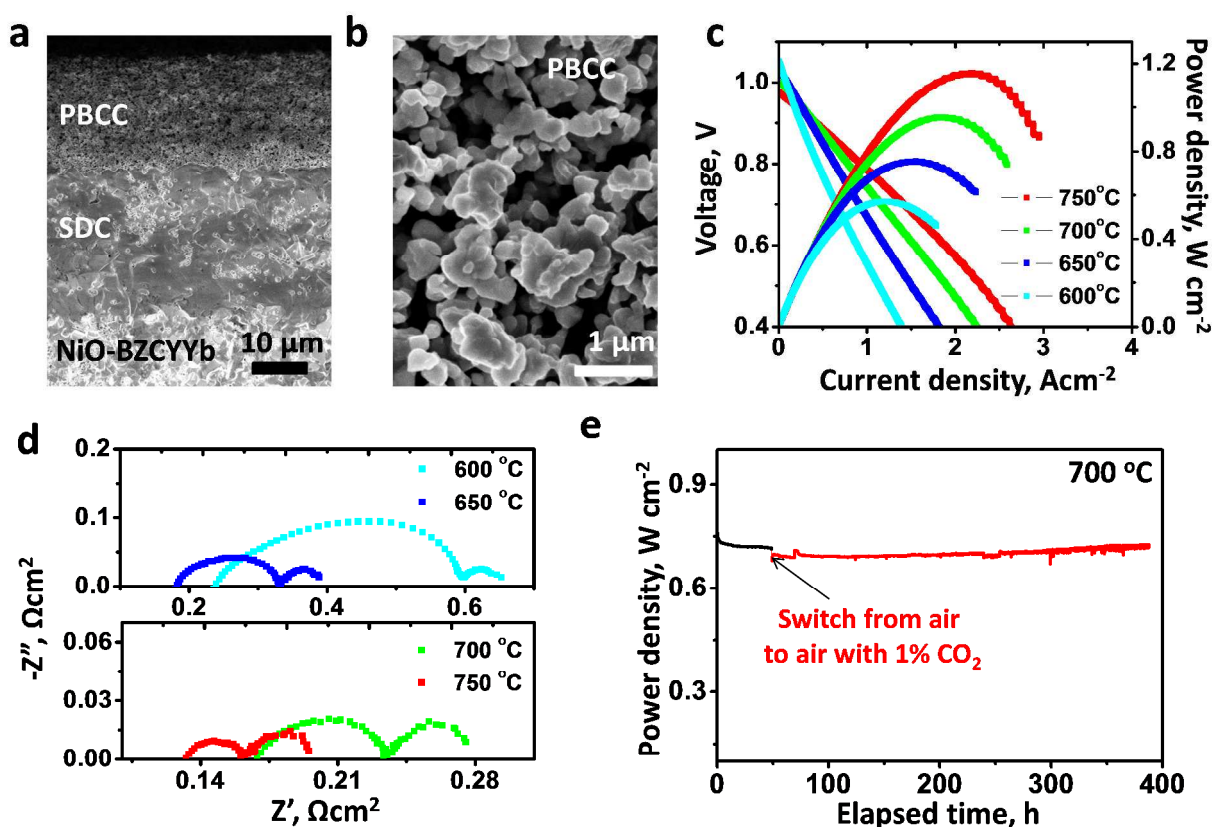


Figure 4 Microstructure and performance of single cells. (a) Typical SEM image of an anode supported cell with a configuration of NiO-BZCYYb anode, SDC electrolyte, and PBCC cathode; (b) Detailed morphology of PBCC cathode; Typical *IVP* curves(c), and EIS (d) of a single cell measured at temperature of 600-750 °C; and (e) Durability of a single cell at voltage of 0.7 V at 700 °C. The cells were fueled by wet H₂ (3% H₂O humidified) in either air or air with 1% CO₂.

Table 1 Summary of electrolyte, thickness of electrolyte, anode/cathode materials, OCV and maximum power density (P_{max}) for recent SOFCs with similar configuration and materials.

Electrolyte	Thickness [μm]	Anode; cathode	OCV [V]	P_{max} [Wcm ⁻²]	Year ^{Ref}
SDC	30	Ni-BZCYYb; LSCF	0.995 (750°C)	0.76 (700°C)	2012 ⁴⁵
SDC	15	Ni-BZY20; SSC-SDC	1.01 (700°C)	0.76 (700°C)	2014 ⁴⁷

SDC	13	Ni-BZCY; SSC-SDC	1.04 (700°C)	1.006 (700°C)	2014 ⁴⁶
SDC	15	Ni-SCYb; SSC	0.96 (650°C)	0.478 (650°C)	2017 ⁴⁹
GDC	~30	Ni-BZCG; SSC-SDC	1.0 (650°C)	0.45 (650°C)	2015 ⁵⁰
GDC BZG GDC	~30	Ni-SDC;	0.96 (600°C)	0.25 (600°C)	2008 ⁵¹
SDC	~20	Ni-BaMn _{1-x} Ni _x O ₃ -SDC; SSC-SDC	1.01 (650°C)	0.62 (650°C)	2018 ⁵²
SDC	30	Ni-BZCYYb; PBCC	1.00 (700°C); 1.03 (650°C)	0.949 (700°C); 0.72 (650°C)	This work

Note: BZCY: BaZr_{0.1}Ce_{0.7}Y_{0.2}O_{3-δ}; BZY20: BaZr_{0.8}Y_{0.2}O_{3-δ}; SSC: Sm_{0.5}Sr_{0.5}CoO_{3-δ}; SDC: Ce_{0.8}Sm_{0.2}O_{2-δ}; SCYb: SrCe_{0.95}Yb_{0.05}O_{3-δ}; BZCG: BaZr_{0.45}Ce_{0.45}Gd_{0.1}O₃; BCG: BaCe_{1-x}Gd_xO_{3-d}

Understanding of excellent CO₂-tolerance of PBCC

In order to gain deeper understanding of the robust surface properties of PBCC, we have fabricated dense PBCC thin films via pulsed laser deposition (PLD), and investigated the surface evolution as a function of exposure time to a gas mixture with 10% CO₂ and 90% O₂ using *in situ* Raman spectroscopy, which is a powerful tool for probing chemical and physical properties of electrode materials. By simultaneously performing electrochemical and Raman measurements, the chemical and structural evolution of electrode materials under practical operating conditions can be acquired as a function of external stimuli (e.g., current, voltage, partial pressure of CO₂). However, the low signal intensity of Raman spectroscopy makes it difficult to detect the surface species present in trace amount or to track the formation of surface species with short lifetimes. This problem becomes more severe when studying SOFCs materials under realistic operating conditions (ROC) because many ceramic phases possess weak Raman modes and all Raman peaks broaden at high temperatures. Surface enhanced Raman scattering (SERS) is a promising solution to this problem. In addition, a model cell with a high quality thin-film working electrode was used for this fundamental micro-spectroscopic study since well-controlled electrode geometry can rule out the uncertainties caused by variations in morphology. Schematically shown in **Figure 5a** is the experimental set-up and the model electrode configuration for our *in*

in situ SERS measurements. Either LSCF or PBCC thin-film electrode was deposited on a single crystal YSZ substrate using a pulsed laser deposition (PLD) technique³. The highly textured PLD films of PBCC and LSCF, grown on YSZ single crystal (001), are mainly with orientation of (001), as shown in **Figure S4-S5**. Dense and flat PLD films are expected to provide more reliable information on surface properties by excluding the uncertainties associated with morphology and crystal orientation. An SDC thin film buffer layer was applied to avoid possible reaction between the electrode and the YSZ electrolyte. The structure of the LSCF or the PBCC was probed as a function of time exposed to an atmosphere of pure O₂ or O₂ with 10% CO₂ at 500 °C. The two samples were exposed to pure O₂ at 500°C before exposure to CO₂. As shown in **Figure 5b**, the Raman spectra of the LSCF film are featureless in pure O₂, while the peaks of carbonates at ~1060 cm⁻¹ increased drastically after switching the gas from pure O₂ to O₂ with 10% CO₂. However, the carbonate peaks in the Raman spectra of the PBCC sample were undetectable, indicating that PBCC may not react with CO₂ even when the concentration of CO₂ is as high as 10%. Shown in **Figure 5c** are the SEM images of the LSCF and the PBCC thin films before and after exposure to 10% CO₂ (taken from the Raman chamber). While the LSCF thin film became much rougher after exposure to CO₂, the PBCC thin film remained almost unchanged. **Figure 5d** is the variation in intensity of the carbonate peaks obtained from thin films of LSCF or PBCC at 500 °C as a function of time. It demonstrates that the PBCC electrode material is not affected by the exposure to CO₂. We also prepared dense pellets of PBCC and LSCF using a traditional high-temperature sintering process and performed *in situ* SERS measurements under the identical conditions. It is clearly shown that the trend of Raman spectra evolution of the PBCC pellets is similar to that of the PLD PBCC thin films (**Figure S6**). These results clearly confirm

that the PBCC surface is much more robust against CO_2 than the LSCF surface, consistent with the XRD analysis and the electrochemical measurements of the PBCC electrode discussed earlier.

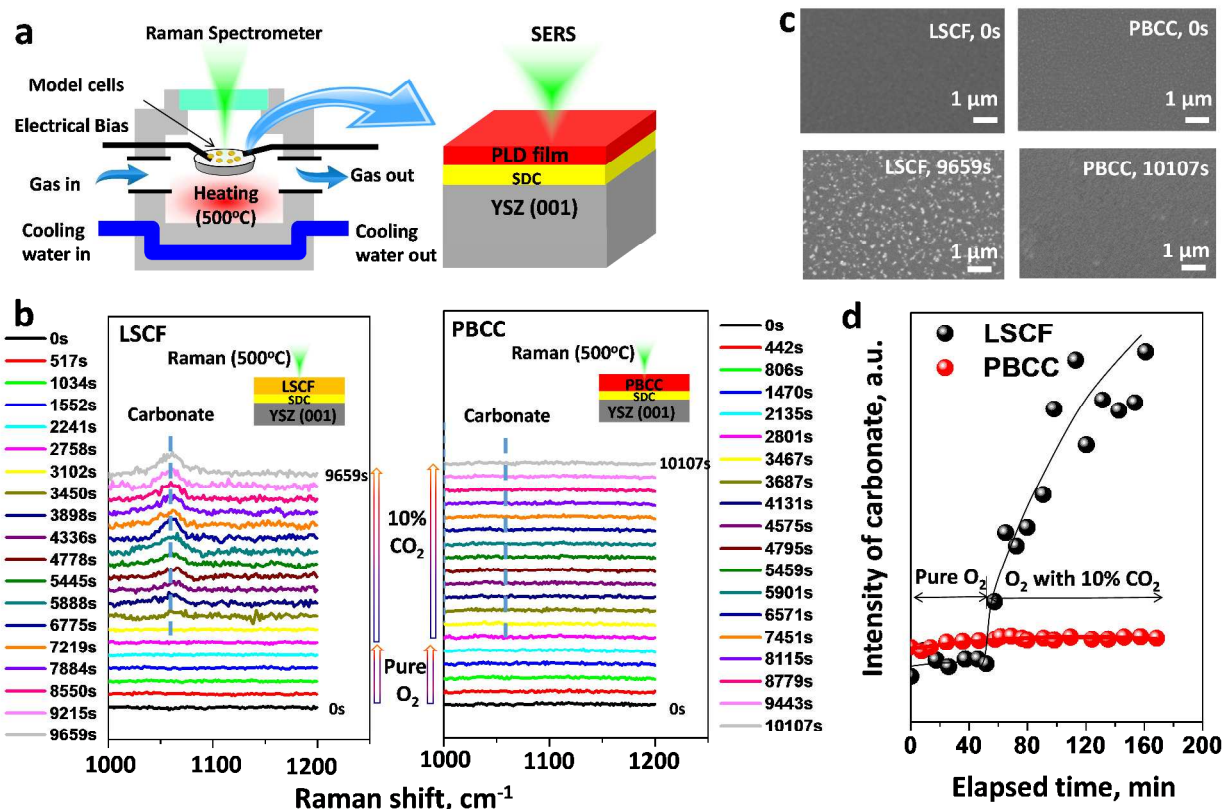


Figure 5 *In situ* Surface enhanced Raman spectroscopic (SERS) study of thin film electrode prepared by PLD.

(a) Schematics of *in situ* SERS study; (b) *In situ* SERS spectra of LSCF and PBCC thin film at 500 °C in atmosphere of pure O_2 or O_2 with 10% CO_2 ; (c) SEM of fresh films and films after Raman testing in O_2 with 10% CO_2 ; (d) Intensity of carbonate peak of ($\sim 1060\text{cm}^{-1}$) observed from thin film LSCF and PBCC surface.

To gain more insights into the carbonate formation on the LSCF and PBCC surfaces at the molecular level, we resorted to DFT calculations. Due to various metal-oxide terminations, we first performed a thermodynamic analysis by calculating the heat of reactions with available heat of formation data in the literature as compiled in **Table S1**. It shows that the carbonate formation can more easily occur from Co and Fe ions (631.5 – 665.6 kJ/mol) rather than Ca, Ba, or Sr ions (941.7 – 1028.6 kJ/mol). However, these results could not explain the growth of the

carbonate peak observed in the SERS at $\sim 1060\text{ cm}^{-1}$. Accordingly, DFT calculations were carried out to precisely explain why PBCC is inactive for the carbonate formation. In this study, the (010) surfaces were used as we applied the (010) plane of double-layered perovskite structures in which pore channels could be formed to enhance the bulk diffusion^{3, 53}. Based on the bulk structures of LSCF and PBCC illustrated in **Figure S7**, we calculated CO_2 adsorption energies on the LSCF and PBCC surfaces. For these initial calculations, we considered the CoO-terminated PBCC surface and LaSrO- and CoFeO-terminated LSCF surfaces as shown in **Figure S8**. Surface energy calculation of LaSrO- and CoFeO-terminated LSCF shows that they are indistinguishable (-1.03 and -1.06 J/m^2 , respectively). Thus, we examined CO_2 adsorption on the two terminations of LSCF. The side views of CO_2 adsorption on the surfaces are illustrated in **Figure 6**. As compiled in **Table S2**, the adsorption energy calculations clearly support the experimental findings that PBCC has much weaker adsorption of CO_2 than LSCF (-0.73 eV versus -1.25 eV , respectively). This weak interaction between CO_2 and the PBCC's surface compared to LSCF may effectively inhibit the carbonate formation under the fuel cell conditions. This is in line with the experimental finding that PBCC does not uptake CO_2 . In addition to the adsorption energy comparison, we examined the geometrical change in more detail, as shown in **Figure 6**. Only LaSrO-terminated LSCF(010) has a complete CO_3^{2-} formation, while other adsorptions on CoO- or CoFeO-terminated surfaces are molecular CO_2 adsorption. In addition, it was found that the oxygen vacancy affects the CO_2 adsorption energy on LaSrO-terminated LSCF(010), leading to a more complete carbonate formation. It increases the adsorption energy from -1.25 eV to -2.23 eV . On the basis of the surface calculations, we carried out further simulations to understand the growth of the characteristic Raman peak at $\sim 1060\text{ cm}^{-1}$ as a function of CO_2 treatment time, as shown in **Figure 5**. For this examination, the DMol³ module

implemented in the Materials Studio package was applied. The LaSrO-terminated LSCF (010) was chosen for the single-point energy calculations. As illustrated in **Figure S9**, two surface coverages of CO₂ adsorption (i.e., CO₂ = 2 and 4), resulting in the Raman activities of 0.13 and 0.51 A⁴/amu, respectively, formed at ~1,064 cm⁻¹ and ~1,056 cm⁻¹, respectively. These characteristic Raman peaks were scaled by a factor of 0.8497 which was obtained by comparing the experimental characteristic Raman peak of bulk SrCO₃⁵⁴ and the predicted value in this study (1069 cm⁻¹ versus 1210 cm⁻¹, respectively). This result clearly supports the growth of the carbonate's Raman characteristic peak at ~1,060 cm⁻¹. Since it is well known that the dopant Sr ions from LSCF are segregated to the surface rather than La ions, we simulated two layers of CO₃²⁻ formation on LaSrO-terminated LSCF (010) (see **Figure 6e**, **Figure S10**), resulting in the Raman activity of 0.33 A⁴/amu at ~1,062 cm⁻¹. For this calculation, the La ions on the top-most layer were replaced by Sr ions. The two different types of the carbonate formation on the surface clearly manifest that the growth of our SERS data at ~1060 cm⁻¹ results from the carbonate formation by the strong interaction of CO₂ and the LSCF cathode materials, while PBCC is effectively designed to be CO₂-tolerant under fuel cell conditions.

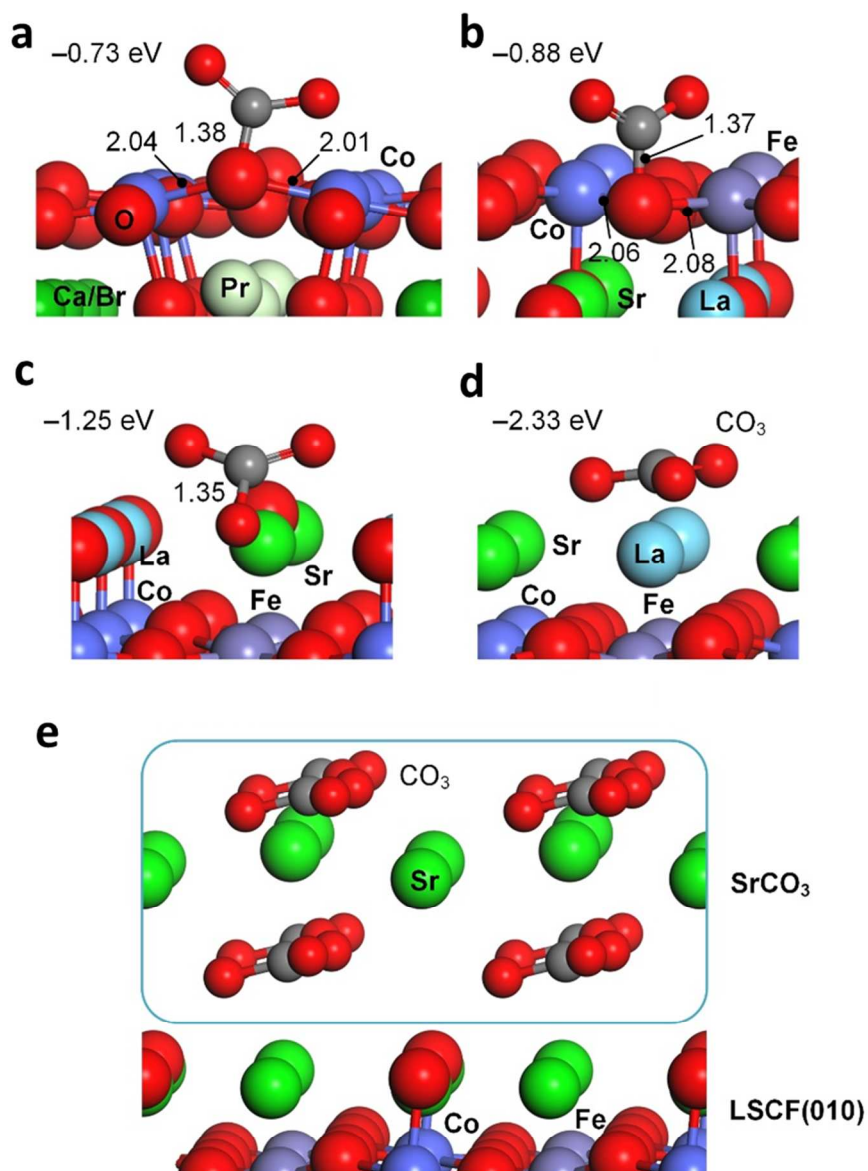


Figure 6 Geometrical illustration of CO₂ adsorption on (a) CoO-terminated PBCC(010), (b) CoFeO-terminated LSCF(010) without an oxygen vacancy, (c) LaSrO-terminated LSCF(010) without an oxygen vacancy, (d) LaSr-terminated LSCF(010) with an oxygen vacancy, and (e) SrCO₃-formed on LSCF(010). The values are bond lengths in Å.

Conclusion

In summary, a layered double perovskite PrBa_{0.8}Ca_{0.2}Co₂O_{5+δ} (PBCC) cathode, with an excellent ORR activity and CO₂ tolerance, has been fabricated and evaluated in both symmetrical

and single cell configurations under realistic operating conditions. The PBCC cathode exhibited high catalytic activity for ORR with area specific resistance as low as $0.024 \Omega\text{cm}^2$ at 750°C . The analyses of electrochemical impedance spectra as well as *in situ* SERS indicated that the surface of PBCC is much more active for oxygen exchange but robust against CO_2 poisoning than that of LSCF. The PBCC-based materials may also be applicable to other chemical and energy transformation systems that involve oxygen electrochemistry, including electrolysis of CO_2 , gas sensors, oxygen pumps, oxygen separation, and membrane reactors.

Experimental Section

Experimental details can be found in Supporting information.

Conflicts of interest

There are no conflicts of interest to declare.

Acknowledgements

This work was supported by the US Department of Energy SECA Core Technology Program (under award numbers FC FE0026106 and FC-FE0009652) and Guangdong Innovative and Entrepreneurial Research Team Program (No. 2014ZT05N200). This research used resources of the National Energy Research Scientific Computing Center, a DOE Office of Science User Facility supported by the Office of Science of the U.S. Department of Energy under Contract No. DE-AC02-05CH11231.

Reference

1. L. Yang, S. Wang, K. Blinn, M. Liu, Z. Liu, Z. Cheng and M. Liu, *Science*, 2009, **326**, 126-129.

2. L. Yang, Y. Choi, W. Qin, H. Chen, K. Blinn, M. Liu, P. Liu, J. Bai, T. A. Tyson and M. Liu, *Nat Commun*, 2011, **2**, 357.
3. Y. Chen, Y. Chen, D. Ding, Y. Ding, Y. Choi, L. Zhang, S. Yoo, D. Chen, B. deGlee, H. Xu, Q. Lu, B. Zhao, G. Vardar, J. Wang, H. Bluhm, E. J. Crumlin, C. Yang, J. Liu, B. Yildiz and M. Liu, *Energy Environ. Sci.*, 2017, **10**, 964-971.
4. Y. Chen, Y. Choi, S. Yoo, Y. Ding, R. Yan, K. Pei, C. Qu, L. Zhang, I. Chang, B. Zhao, Y. Zhang, H. Chen, Y. Chen, C. Yang, B. deGlee, R. Murphy, J. Liu and M. Liu, *Joule*, 2018, **2**, 938-949..
5. Z. Shao and S. M. Haile, *Nature*, 2004, **431**, 170-173.
6. M. Liu, M. E. Lynch, K. Blinn, F. M. Alamgir and Y. Choi, *Materials Today*, 2011, **14**, 534-546.
7. Y. Chen, Y. Lin, Y. Zhang, S. Wang, D. Su, Z. Yang, M. Han and F. Chen, *Nano Energy*, 2014, **8**, 25-33.
8. W. Zhou, J. Sunarso, M. Zhao, F. Liang, T. Klande and A. Feldhoff, *Angew. Chem. Int. Ed.*, 2013, **52**, 14036-14040.
9. S. P. Jiang, *Solid State Ionics*, 2002, **146**, 1-22.
10. J. A. Lane, S. J. Benson, D. Waller and J. A. Kilner, *Solid State Ionics*, 1999, **121**, 201-208.
11. J.-W. Lee, Z. Liu, L. Yang, H. Abernathy, S.-H. Choi, H.-E. Kim and M. Liu, *J Power Sources*, 2009, **190**, 307-310.
12. J. E. O'Brien, C. M. Stoots, J. S. Herring and J. J. Hartvigsen, 2005.
13. W. Lee, J. W. Han, Y. Chen, Z. Cai and B. Yildiz, *J. Am. Chem. Soc.*, 2013, **135**, 7909-7925.
14. S. P. Jiang, S. Zhang and Y. D. Zhen, *J. Electrochem. Soc.*, 2006, **153**, A127-A134.
15. S. Y. Lai, D. Ding, M. Liu, M. Liu and F. M. Alamgir, *ChemSusChem*, 2014, **7**, 3078-3087.
16. Y. Chen, S. Yoo, X. Li, D. Ding, K. Pei, D. Chen, Y. Ding, B. Zhao, R. Murphy, B. deGlee, J. Liu and M. Liu, *Nano Energy*, 2018, **47**, 474-480.
17. Z. Jiang, C. Xia and F. Chen, *Electrochim. Acta*, 2010, **55**, 3595-3605.
18. S. P. Jiang, *Int. J. Hydrogen Energy*, 2012, **37**, 449-470.
19. J. M. Vohs and R. J. Gorte, *Adv Mater*, 2009, **21**, 943-956.
20. N. Tsvetkov, Q. Lu, L. Sun, E. J. Crumlin and B. Yildiz, *Nat Mater*, 2016, **15**, 1010-1016.
21. S. P. Jiang and X. Chen, *Inter. J. Hydrogen Energy*, 2014, **39**, 505-531.
22. Y. D. Zhen and S. P. Jiang, *J. Electrochem.Soc.*, 2006, **153**, A2245-A2254.
23. L. Zhao, S. Amarasinghe and S. P. Jiang, *Electrochem. Commun.*, 2013, **37**, 84-87.
24. K. Chen, N. Ai, K. M. O'Donnell and S. P. Jiang, *Phy. Chem. Chem. Phy.*, 2015, **17**, 4870-4874.
25. D. Ding, X. Li, S. Y. Lai, K. Gerdes and M. Liu, *Energy Environ. Sci.*, 2014, **7**, 552-575.
26. W. Zhou, F. Liang, Z. Shao and Z. Zhu, *Sci. Rep.*, 2012, **2**, 327.
27. Y. Zhu, W. Zhou, Y. Chen and Z. Shao, *Angew. Chem. Int. Ed.*, 2016, **55**, 8988-8993.
28. T. Komatsu, H. Arai, R. Chiba, K. Nozawa, M. Arakawa and K. Sato, *Electrochem. Solid-State Lett.*, 2006, **9**, A9-A12.
29. X. D. Zhou, J. W. Templeton, Z. Nie, H. Chen, J. W. Stevenson and L. R. Pederson, *Electrochim. Acta*, 2012, **71**, 44-49.
30. S. Yoo, A. Jun, Y.-W. Ju, D. Odkhoo, J. Hyodo, H. Y. Jeong, N. Park, J. Shin, T. Ishihara and G. Kim, *Angew. Chem. Int. Ed.*, 2014, **53**, 13064-13067.
31. S. Sengodan, S. Choi, A. Jun, T. H. Shin, Y.-W. Ju, H. Y. Jeong, J. Shin, J. T. S. Irvine and G. Kim, *Nat Mater*, 2015, **14**, 205-209.
32. A. Chroneos, D. Parfitt, J. A. Kilner and R. W. Grimes, *J Mater Chem*, 2010, **20**, 266-270.
33. Y. Chen, Y. Bu, B. Zhao, Y. Zhang, D. Ding, R. Hu, T. Wei, B. Rainwater, Y. Ding, F. Chen, C. Yang, J. Liu and M. Liu, *Nano Energy*, 2016, **26**, 90-99.
34. A. A. Taskin, A. N. Lavrov and Y. Ando, *Applied Physics Letters*, 2005, **86**, 091910.
35. G. Kim, S. Wang, A. Jacobson, L. Reimus, P. Brodersen and C. Mims, *J Mater Chem*, 2007, **17**, 2500-2505.

36. J. H. Kim, M. Cassidy, J. T. S. Irvine and J. Bae, *J. Electrochem. Soc.*, 2009, **156**, B682-B689.
37. J. G. Lee, J. H. Park and Y. G. Shul, *Nat Commun*, 2014, **5**.
38. Y. Chen, Y. Bu, Y. Zhang, R. Yan, D. Ding, B. Zhao, S. Yoo, D. Dang, R. Hu, C. Yang and M. Liu, *Adv. Energy Mater.*, 2017, **7**, 1601890.
39. Y. Zhang, Y. Chen and F. Chen, *J. Power Sources*, DOI: <http://dx.doi.org/10.1016/j.jpowsour.2014.11.123>.
40. J.-D. Kim, G.-D. Kim, J.-W. Moon, Y.-i. Park, W.-H. Lee, K. Kobayashi, M. Nagai and C.-E. Kim, *Solid State Ionics*, 2001, **143**, 379-389.
41. J. Wang, L. Jiang, X. Xiong, C. Zhang, X. Jin, L. Lei and K. Huang, *J. Electrochem. Soc.*, 2016, **163**, F891-F898.
42. M. Li, Y. Ren, Z. Zhu, S. Zhu, F. Chen, Y. Zhang and C. Xia, *Electrochim. Acta*, 2016, **191**, 651-660.
43. Z. Jiang, Z. Lei, B. Ding, C. Xia, F. Zhao and F. Chen, *Int. J. Hydrogen Energy*, 2010, **35**, 8322-8330.
44. Y. Takeda, R. Kanno, M. Noda, Y. Tomida and O. Yamamoto, *J. Electrochem. Soc.*, 1987, **134**, 2656-2661.
45. M. Liu, D. Ding, Y. Bai, T. He and M. Liu, *J. Electrochem. Soc.*, 2012, **159**, B661-B665.
46. W. Sun and W. Liu, *J Power Sources*, 2012, **217**, 114-119.
47. W. Sun, Z. Shi, J. Qian, Z. Wang and W. Liu, *Nano Energy*, 2014, **8**, 305-311.
48. Z. Shao, W. Zhou and Z. Zhu, *Prog. Mater. Sci.*, 2012, **57**, 804-874.
49. Z. Gong, W. Sun, J. Cao, Y. Wu, L. Miao and W. Liu, *J. Mater. Chem. A*, 2017, **5**, 12873-12878.
50. J. Cao, Z. Gong, J. Hou, J. Cao and W. Liu, *Ceram Int*, 2015, **41**, 6824-6830.
51. A. Tomita, Y. Tachi and T. Hibino, *Electrochem. Solid-State Lett.*, 2008, **11**, B68-B70.
52. J. Qian, Z. Gong, M. Wang, H. Yu, T. Zhao, M. Li, W. Liu and H. Wang, *Ceram Int*, 2018, **44**, 12739-12744.
53. S. Choi, S. Yoo, J. Kim, S. Park, A. Jun, S. Sengodan, J. Kim, J. Shin, H. Y. Jeong, Y. Choi, G. Kim and M. Liu, *Sci. Rep.*, 2013, **3**, 2426.
54. P. Colomban, C. Tran, O. Zaafrani and A. Slodczyk, *J. Raman Spectro.*, 2013, **44**, 312-320.